Ultrasonics Sonochemistry 112 (2025) 107187

Contents lists available at ScienceDirect

Ultrasonics Sonochemistry

journal homepage: www.elsevier.com/locate/ultson

Lamellarity of ultrasound assisted formations of dipalmitoyl-lecithin vesicles

Attila Bóta [a,*], Heinz Amenitsch [b], András Wacha [a]

[a] Research Centre for Natural Sciences, Institute of Materials and Environmental Chemistry, Magyar tudósok körútja 2, 1117 Budapest, Hungary
[b] Austrian SAXS beamline@ELETTRA, Italy and Inorganic Chemistry, Graz University of Technology, Are Science Park 34149 Basovizza TS, Trieste, Stremayrgasse 9, 8010 Graz, Austria

ARTICLE INFO

Keywords:
Ultrasonication
Ultrasound induced unilamellar vesicle
Phase-transition
Bilayered phospholipid fragment
MLV to ULV transformation
Time-resolved in situ SAXS

ABSTRACT

Formation of unilamellae of fully hydrated dipalmitoylphosphatidylcholine (DPPC) was induced by a horn sonicator from multilamellar vesicles and followed by time-resolved synchrotron small angle X-ray scattering and direct visual morphological investigations by the means of transmission electron-microscopy combined with freeze-fracture. Without incubation the ultrasonication causes continuous increasing in temperature and transformation from the gel to rippled gel structures, then reaching the main transition, the formfactor of unilamellar structure appeared. The ultrasonication resulted in different layer formations at the characteristic temperatures of the gel (20 °C), rippled gel (38 °C), and liquid crystalline (45 °C) phases of the system. At 20 °C irregular stacks of multi and oligolamellar lamellae were shaped even after three hours of ultrasonication. At 38 and 45 °C the ultrasound induced dominantly unilamellar vesicles (ULVs) in a short time (10 and 3 – 5 min, respectively, under typical ultrasound treatments in the general laboratory practice). After the end of the ultrasonication, irregular layer formations with defects structures increased when the temperature of sonication was above the chain melting temperature of the hydrated DPPC system, underlining the importance of optimized sonication processes.

1. Introduction

Unilamellar vesicles (ULVs) are of great importance in several fundamental and technological areas connecting to biology, medicine, pharmaceutics, and food technologies [1–6]. However, lipids self-assemble spontaneously into multilamellar vesicles (MLVs) upon hydration, which need to be subsequently transformed into ULVs [7]. This is typically achieved by ultrasonication [8–13], as well as other well-known methods such as extrusion [14], detergent dialysis [15], alcohol injection [16], microfluidic method [17], and supercritical fluid assisted technology [18].

Ultrasonication of the lipid suspension results in acoustic cavitation, producing micro-bubbles [19]. The implosion of these causes high local temperatures and pressures, and creates free hydroxyl and hydrogen radicals [20]. Although the high temperature also accelerates the hydrolysis of phospholipids, this effect is typically negligible. It was found that only 1.6 % of the lipids hydrolysed during a prolonged, 24 h incubation at 50 °C [21]. The typical degradation products of natural lecithins are lysolecithins, fatty acids, glyceryl phosphorylcholine, phosphorylcholine [22].

Ultrasound treatment destroys the integrity of multilamellae, forming temporary products, the so-called bilayered phospholipid fragments (BLFs) [23]. These subsequently rearrange mostly into unilamellar forms.

The dipalmitoyl-lecithin DPPC (1,2-dipalmitoyl-*sn*-glycero-3-phosphocholine) is not a typical lipid component of systems which are generally subjected to ultrasonication in industry. However, it has a well-established and −studied thermotropic behaviour, with obvious morphological and nano-structural characteristics (for a summary, see Section 1 of the Supporting Information to this article). Additionally, DPPC is a widespread biological model membrane-constituent used in biochemical and biophysical studies, and it is a significantly more resistant artificial lipid against ultrasonication than other lipids or lipid mixtures with biological origins [24].

The effectiveness of ultrasonication in turning MLVs into ULVs is generally investigated by the means of dynamic light scattering (DLS), although this method, reporting only an overall size of the vesicles, is clearly unable to describe their lamellar structure [9,10,25]. Imaging

* Corresponding author.
E-mail address: bota.attila@ttk.hu (A. Bóta).

https://doi.org/10.1016/j.ultsonch.2024.107187
Received 5 June 2024; Received in revised form 22 November 2024; Accepted 1 December 2024
Available online 12 December 2024

techniques such as cryo-electron microscopy (Cryo-EM) [26], transmission electron-microscopy combined with freeze-fracturing sample preparation (FF-TEM) [27] and atomic force microscopy (AFM) [28] provide direct and detailed visual information about the morphology of the entirety of vesicles and their shell structures. Apart from the fact that invasive sample preparation procedures are required which can induce significant structural changes, the statistical relevance of these single-particle methods, however, is generally low and prone to human bias. On the other hand, these methods, especially FF-TEM, offer unique insights, whereby local structural changes caused by sonication can be inspected during the whole course of the transformation from MLV to ULV [29,30]. Small-angle X-ray and neutron scattering (SAXS and SANS) methods provide reliable characterization of shape, size and other nanostructural features, but since the experimental results are in reciprocal space, advanced analysis techniques and modelling is often required [31,32]. Fortunately, the small-angle scattering of MLVs and ULVs is highly different, therefore an easy differentiation between the multilamellar and unilamellar forms becomes possible at first glance. In contrast to visible light scattering, here the inner lamellar structure of vesicles can also be deduced, not only their overall size [33].

Another, frequently neglected aspect of ultrasonication is temperature. The consequences of the thermotropic phase behaviour of lipid suspensions are often not taken into account. Temperature control is reported in the literature in a diverse manner. Some authors performed sonication of hydrated phosphatidylcholines, especially dipalmitoylphosphatidylcholine, at the characteristic temperature of the gel phase (25 °C) [34]. Others conducted their measurement in a wide temperature range ("between 25–40 °C", covering the pretransition range) [9]. Yet others only avoid high temperatures ("below 50 °C", allowing the chain melting transition) [10]. Some papers conclude that the phase state of the system (gel or liquid crystalline phase) is not the driving factor of the rapid small unilamellar vesicle formation [11].

In this work we performed an *in operando* study of the ultrasonication process of multilamellar vesicles using an in-line experimental setup where the ultrasonicated lipid suspension is studied with synchrotron small-angle X-ray scattering (SAXS) over the whole course of the ultrasound treatment. As a non-destructive method, SAXS can give unambiguous information on the lamellarity of the lipid vesicles, without any unwanted structural changes due to additional sample preparation steps. The originally observable, several orders of equidistant Bragg reflections that are characteristic for the periodic arrangement of the bilayers in MLVs, transform into a single broad peak, the so-called form factor of a single bilayer, over the course of the ultrasound treatment. Because the small-angle scattering of MLVs carries information also on the thermotropic phases the lipid suspension is in, our experimental setup, extended with a precise temperature control, and also enabled us to devise the role of the gel or liquid crystalline phases in ultrasound-induced unilamellarization. Thereby, we intend to show how thermal circumstances influence the lamellarity of the vesicles under typical ultrasound treatments in the general laboratory practice [10].

2. Material and methods

2.1. Chemicals

DPPC (1,2-dipalmitoyl-*sn*-glycero-3-phosphocholine) was purchased from Avanti Polar Lipids (United States) and were used without further purification. In preparing the MLVs, first a small amount of water was added dropwise to the lipid, yielding a homogeneous, concentrated suspension, approximately 15 w/w %. This form was frequently vortexed and homogenised by repeating a heating (50 °C) and cooling (4 °C) cycle twenty times. Finaly, this form was diluted to the desired 1.5 w/w % concentration.

Physiological salt solution (9 g NaCl solved in 991 g Millipore water) was used for erythrocyte isolation and purification. Their membranes were prepared in hypotonic TRIS buffer medium (5.0 mM TRIS, pH: 7.6). The final haemoglobin free erythrocyte membrane, known as ghost, was stored in PBS buffer (10 mM; 8 g NaCl, 0.2 g KCl, 1.8 g $Na_2HPO_4{\cdot}2H_2O$, 0.312 g $NaH_2PO_4{\cdot}2H_2O$ for 1 L PBS solution, the final pH = 7.4 value was adjusted by HCl). All listed salts were purchased from Sigma Aldrich.

2.2. Preparation of erythrocyte ghost and nanoerythrosomes

Freshly collected anticoagulated blood was donated by healthy volunteers, 18 ml from one donor at a time using 6 ml K3EDTA tubes (Vacuette, Greiner Bio-One, Austria). The use of human blood samples was approved by the Scientific Ethics Committee of the Hungarian Health Scientific Council (ETT TUKEB 6449-2/2019).

Cellular components were sedimented from whole blood by centrifugation (2200 × g, 15 min, swing-out rotor, 14 mL Eppendorf tube, Hermle Z327 K centrifuge, Germany). The plasma and the white blood cell containing buffy coat were removed and the erythrocyte pellet was suspended in physiological NaCl solution and washed three times. After the last sedimentation, the red blood cells were lysed in hypotonic 5 mM TRIS buffer, stirred in 40 × buffer volume at 4 °C. The erythrocyte ghost membrane was sedimented with a Beckman Avanti J-25 I centrifuge, US (JA-20 rotor, average 34000xg, 30 min, 4 °C). To achieve haemoglobin-free ghosts, the membrane pellet was resuspended in hypotonic TRIS buffer again, and centrifuged. Afterwards it was washed in PBS buffer two times and centrifuged (Beckman, Avanti J-25 I centrifuge centrifuge, US, average 34000x g, 30 min, 16 °C).

The final ghost membrane pellet was suspended in PBS, its protein content was determined by Bradford protein assay and was used as a stock solution for nanoerythrosome preparation. The ghost membrane aliquots were rapidly frozen in liquid nitrogen and stored at approx. −80 °C.

The haemoglobin-free ghost was the starting material for nanoerythrosome preparation. The membrane suspension was put in a bath sonicator (Elmasonic S10, 30 W) in glass vial for 10 s, with pre-set power level and continuous operation (37 kHz, in 1.5 ml glass vial, sample volume 200 µl). This gently sonicated ghost suspension was mixed with an amount of DPPC ULVs to reach a final 5:1 DPPC to ghost mass ratio. The mixture was vortexed and sonicated (Elmasonic bath sonicator, 20 s) and extruded using Mini Extruder (Avanti Lipids, Al, US) sequentially through membranes of pore sizes 1000, 400, 200 and finally, 100 nm.

2.3. In situ small-angle X-ray scattering (SAXS)

SAXS measurements were performed at the Austrian SAXS beamline of the Elettra synchrotron (Trieste, Italy) in transmission geometry [35]. For the in-situ study, a special sample environment was constructed, the schema of which is shown in Fig. 1.

6 mL of the lipid suspension was situated in a continuous flow tank reactor, a covered but not closed cylindrical glass vial (diameter 23 mm and height 40 mm), into which the 3.8 mm stepped micro titanium tip of an ultrasonic homogenizer (Model 150VT, 150 Watt, Biologics, Inc., United States) was dipped in a way that the tip was in the rotational axis of the vial. The ultrasound source was driven at 20 kHz, at 35 % of its maximal 150 W power, and set to 25 % duty cycle with a cycle length of 2 s. The timer was set to 15 min. At 38 and 45 °C, shorter sonication times were already efficient within 15 min. At 20 °C (gel phase of hydrated DPPC) 12 × 15 min (three hours) of sonication were applied. After every 15 min, a rapid visual control was taken about the proper function of the experimental setup and the next sonication was started immediately. In the case without thermal incubation, 3 × 15 min of sonication was necessary to reach the expected structural changes and observe them with synchrotron small-angle X-ray scattering.

Two alternative setups were used, one where the sonicated sample was not thermally controlled (Fig. 1, left side) and another where the ultrasonication process was carried out in incubated condition, with the thermostatically controlled sonication cell and the X-ray capillary

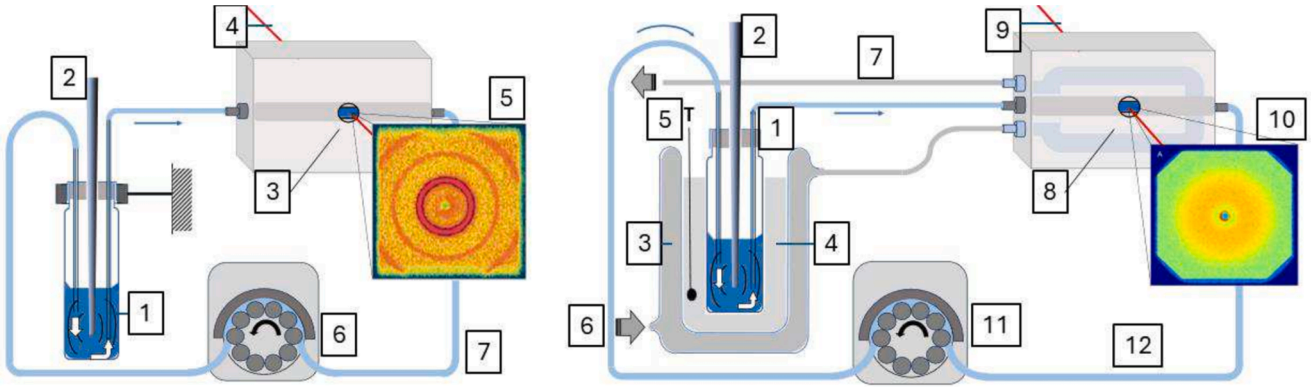

Fig. 1. Scheme of the experimental arrangements. The DPPC suspension was ultrasonicated in the glass tank reactor and circulated through an X-ray capillary by using a peristaltic pump. The sample during the sonication was without incubation (left, tank reactor:1, sonicator tip:2, flow capillary set in metal block:3, X-ray:4, characteristic 2D scattering pattern of MLVs:5, peristaltic pump:6, tube with circulating sample:7) and with incubation (right, tank reactor:1, sonicator tip:2, double-walled vessel for incubation:3, water as intermediary medium:4, temperature control of intermediary medium:5, incubated liquid of the thermostat, inlet:6, incubated liquid of the thermostat, outlet:7, incubated flow capillary set in metal block:8, X-ray:9, characteristic 2D scattering pattern of ULVs:10, peristaltic pump:11, tube with circulating sample:12).

(Fig. 1, right side). In the latter one, the experiments were executed at different temperatures which are relevant to the thermotropic phases of the DPPC/water system: 20 °C (gel phase), 38 °C (rippled gel phase), and 46 °C (liquid crystalline phase) [36–39].

Measurements were done using monochromatized and collimated radiation of 8 keV photon energy. The scattering patterns were recorded in the range of 0.1–5 nm^{-1} in terms of the scattering variable, q (defined as $q = \frac{4\pi}{\lambda}\sin\theta$, where 2θ is the scattering angle and λ is the X-ray wavelength), using a Pilatus 1 M two-dimensional positive sensitive CMOS hybrid pixel detector (Dectris Ltd, Baden, Switzerland). To be able to assess sample stability during the experiment, twenty exposures, each 1 s long, were made and repeated for each sample. The relevant aqueous medium was measured before and after the measurement series. The individual exposures were corrected for beam flux, geometric effects. The background scattering curve was subtracted in the case of the measurements of nanoerythrosomes. The corrected scattering patterns were azimuthally averaged to yield one-dimensional scattering curves for each sample.

2.4. Transmission electron microscopy combined with freeze fracture (FF-TEM)

For the FF-TEM measurements, the sample was first ultrasonicated at the desired temperature. Then a single droplet, approximately 1 μL, was pipetted onto a golden sample holder and rapidly frozen in liquid freon [40]. Three samples, coming from the different temperatures, were put, together with their sample holders onto the freeze fracture sample holder block, under liquid nitrogen at −195.8 °C. The sample holder block was finally placed into the freeze-fracture device (BAF 400D, Balzers AG, Liechtenstein), where the fracturing was performed at −100 °C under high vacuum. After a short etching (approx. 20 sec) the fractured surfaces of the samples were covered with vaporized platinum, producing the surface masks, and then coated with vaporized carbon to create a continuous supporting film on the stacked platinum masks. Taken out from the vacuum chamber, the replicas were cleaned from the remainders of the samples with distilled water and transferred separately to copper grids (200 mesh) for examination in a transmission electron microscope operating at 80 kV (MORGAGNI 268D, FEI, The Netherlands).

2.5. Dynamic light scattering (DLS)

The average size and size distribution of the samples was measured with a W130i dynamic light scattering apparatus (AvidNano, United Kingdom) [41]. 5 μL of the sample was diluted with 75 μL MQ water and measured in a microcuvette at 20 °C. The analysis of the measurement data was performed with the i-Size software supplied with the apparatus.

3. Results and Discussion

3.1. Structural changes induced by ultrasonication without temperature control

The first measurement series, modelling typical laboratory conditions, was carried out at room temperature (cca. 20 °C), without temperature control. The glass cell used for ultrasonication was not isolated from its environment – it was fixed to a laboratory stand holder –, but the sonication produced a monotonous increase in the temperature of the DPPC suspension up to approx. 46 °C, which was reached in 25 min. The increasing temperature of the sample induced remarkable changes in the SAXS patterns of the system as it can be followed in Fig. 2 A, B. The SAXS curves show the characteristic nanostructures and transitional states thereof, corresponding to the thermotropic behaviour of the hydrated DPPC multilamellar system in the temperature domains of the gel ($L_{\beta'}$) and rippled gel ($P_{\beta'}$) phases [30,38,39,42,43]. As the temperature increased above the main transition, the form factor of the unilamellar structure appeared, instead of the scattering signal of the multilamellar liquid crystalline (L_α) phase.

Under closer inspection, further details can also be revealed from the scattering curves. At the beginning of the ultrasonication (near 20 °C), sharp, equidistant Bragg reflections are detectable, corresponding to the lattice spacing (d = 6.35 nm) of the gel phase ($L_{\beta'}$) via Bragg's equation:

$$d = \frac{2\pi}{q_n}n,$$

where n, an integer, is the order of the peak, q_n is the position of its centre, and d is the periodic repeat distance. As time progresses and temperature increases, the nanostructural signals of thermally adjacent phases appear. First the gel and then the rippled gel ($P_{\beta'}$) phases are observable, with some transient behaviour between them. Finally, ultrasonication results in a general destruction of the regular layer packing of MLVs. Even in the temperature domain of $L_{\beta'}$, a remarkable loss in multilamellar correlation can be observed, through the disappearance of higher order Bragg reflections, showing a second kind of layer defects which affect the relative organization of the lipid bilayers with respect to each other. Above the so-called pre-transition (between the $L_{\beta'}$ and $P_{\beta'}$ phases), the $P_{\beta'}$ phase also did not assume its regular,

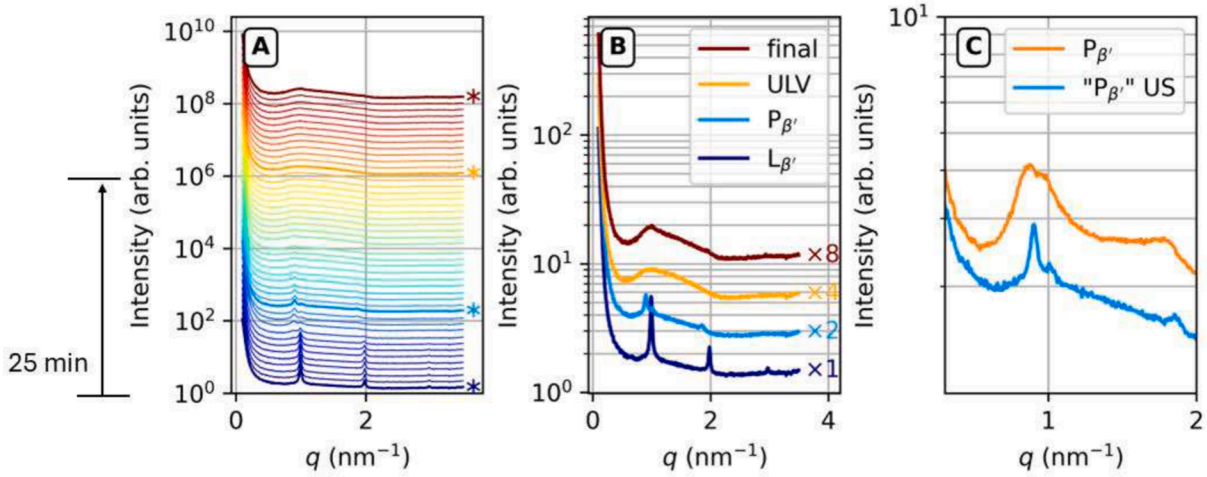

Fig. 2. Changes of the one-dimensional SAXS profiles of hydrated DPPC system (1.5 w/w%) during the sonication process without incubation. The whole course of transformation (A, patterns signed with asterisk are shown in B). Representative SAXS patterns (B). Comparison of the steady state (upper) and dynamic (bottom) forms of $P_{\beta'}$ phase (C).

multilamellar form. The impact of ultrasound seems to be accumulated and caused more extended alterations in this inherently more mobile phase. The Bragg reflections appeared only in two orders, witnessing a further loss in lamellarity. Comparing this "dynamic" SAXS pattern of the $P_{\beta'}$ phase to that of the steady state at 38 °C (measured separately) in Fig. 2C, a difference between the shapes of scattering curves appears, indicating the effect of ultrasound. The diffraction peaks of the $P_{\beta'}$ phase are complex, and this behaviour is the consequence of the two-dimensional surface pattern of the ripple-gel phase, shown in the *Supplementary material 1*. It is noteworthy that in case of the sonicated sample, the Bragg peaks, located at approx. q = 0.88 and 1.00 nm^{-1}, respectively, are sharper and definitely more separated than those of the "true" $P_{\beta'}$ phase, achieved without ultrasonication (bottom and upper curves in Fig. 2C)[44,45]. At the same time, an increased baseline is observable in the whole q-range for the sonicated sample, indicating the scattering of uncorrelated layers. Based on the FF-TEM results sonication breaks up the MLVs already in the early stages of the treatment, producing a significant amount of stand-alone bilayers and weakly correlated layers of stacks of these. The remaining MLVs however remain rather regularly packed. This finding is in full agreement with earlier experimental observations of Zasadzinski (1986), obtained in a model liposomal system by FF-TEM [29]. With increasing temperature, first the second order peak of the $P_{\beta'}$ phase disappears, then the broadened first one dwindles away, giving place to the continuously forming broad, hump-like signal, corresponding to the form factor of the single lipid bilayer of ULVs (Fig. 2A). Due to sonication, the characteristic Bragg reflections of the liquid crystalline phase did not appear. Following the structural changes for 20 mins after the end of ultrasound treatment, a slight but continuous change in the SAXS pattern can be observed, while the sample was cooled down to approx. 25 °C. A small excess, diffuse diffraction signal, centred at the expected position of the $L_{\beta'}$ diffraction, also appears over the bilayer form factor, indicating a partial recombination into a multilamellar arrangement (upper curve in Fig. 2B).

The performed measurements showed that the primary effect of the sonication was the increase in temperature. ULVs were only formed in the higher temperature domain, indicating that the MLV to ULV transformation required a more mobile phase than the rigid gel phase. To observe the impact of ultrasound treatment in distinct phases, further measurements were carried out with temperature control at 20, 38, and 45 °C, which are characteristic for the gel, rippled gel, and liquid crystalline phases of the hydrated DPPC system, respectively [30,39,43].

3.2. Changes of MLVs in gel phase (20 °C)

Fig. 3 shows the effect of sonication onto the multilamellar arrangement of the gel phase ($L_{\beta'}$) at 20 °C. In the beginning, the characteristic Bragg reflections appeared in five orders (three is shown in the Figure), similarly to the previous case where no incubation was used. The position of the first Bragg peaks does not change, not even at prolonged/sustained sonication as it is observable in Fig. 3A. Only the number of the equidistant Bragg peaks is reduced and peaks up to the second order, in form of a shoulder, would be observed after three hours of sonication, indicating a severe loss in correlation and the reduction of the number of layers inside the multilamellar stacks. The changes in the SAXS profiles are highlighted in Fig. 3B, where the starting, a transitional and the final scattering curves are shown. The final SAXS curve indicates extremely weakly correlated MLVs, but the coexistence with ULVs also cannot be precluded.

The FF-TEM pictures (Fig. 4) provide direct visual information about the morphology formed at 20 °C and altered by ultrasonication. In the beginning, the steady state of the DPPC-water system shows large, in some parts onion-like, multilamellar vesicles, where the lamellae exhibit closely packed regular arrangements corresponding to the high number of equidistant Bragg reflections found in the SAXS pattern. Though the lipid concentration is small (1.5 w/w %), complete and relatively large vesicles appear in the aqueous medium. Their size range extends from 0.5 to several μm. The fractured surface morphologies of the vesicles show positive (Fig. 4A) and negative (Fig. 4B) curvatures of the lipid bilayers. In these cases, the fractures occurred in the upper and bottom parts of the embedded vesicles, respectively. In the latter case the closely and regularly packed stacks of bilayer can be observed, giving a picturesque explanation for the series of sharp Bragg reflections. Three hours of sonication induced dramatic changes in the morphology of the lipid-water system (Fig. 4C). Laterally extended anisotropic stacks of lamellae, which seem to be bilayered phospholipid fragments, appear dominantly in the electron-micrographs. Their size lies approximately between 200 and 400 nm, while their thicknesses vary between 100 – 200 nm. Some stacks contain layers in reduced numbers, between two and four, gaps popping up between them, giving explanation for the weak layer correlation observed by the SAXS method. The occurrence of small vesicles is infrequent, suggesting that the formation of closed entities is hindered. The polydisperse particle size distribution profile, obtained by DLS measurement is in line with these observations (Fig. 4D). The shape of the distribution shows a bimodal character, consisting of a relatively sharp peak in the range from 180 until 350 nm,

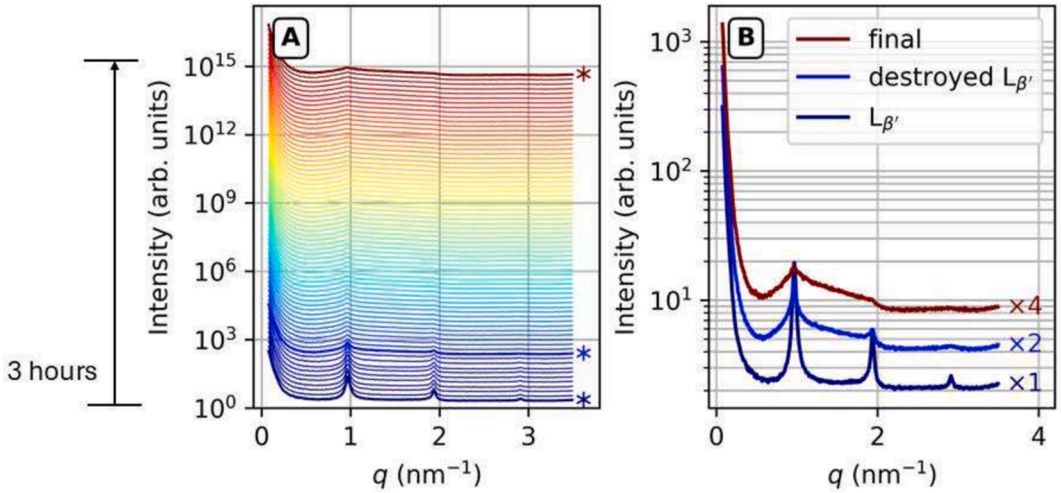

Fig. 3. Changes of the one-dimensional SAXS profiles of hydrated DPPC system (1.5 w/w%) during the sonication process at 20 °C. The whole course of transformation (A, patterns signed with asterisk are shown in B). Representative SAXS patterns (B).

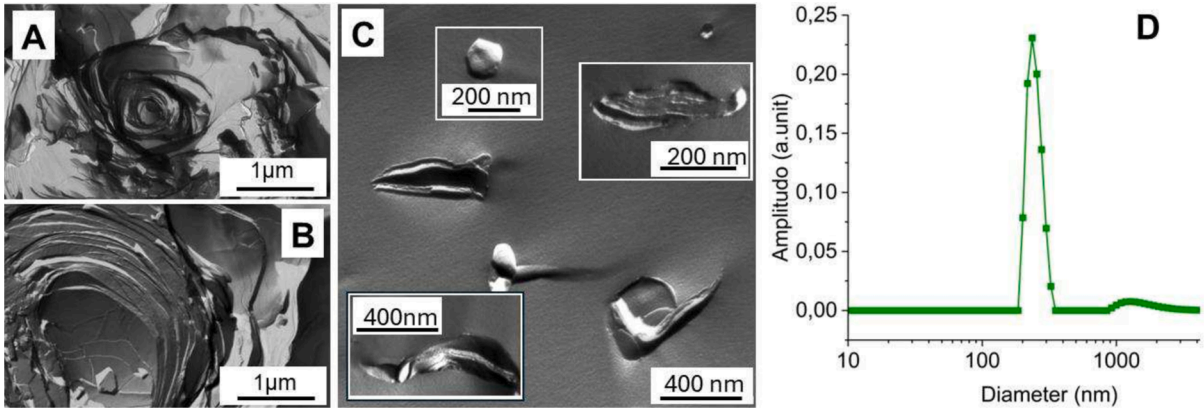

Fig. 4. Surface morphology of the DPPC suspension at 20 °C without ultrasonication (A, B) after ultrasonication (C) and size distribution of the ultrasonicated suspension (D).

and smaller but broadener one, from 0.9 to 3 μm. The PDI values are 0.45 and 0.73, respectively. The second high PDI value indicates that the larger objects probably are not suitable for DLS characterization.

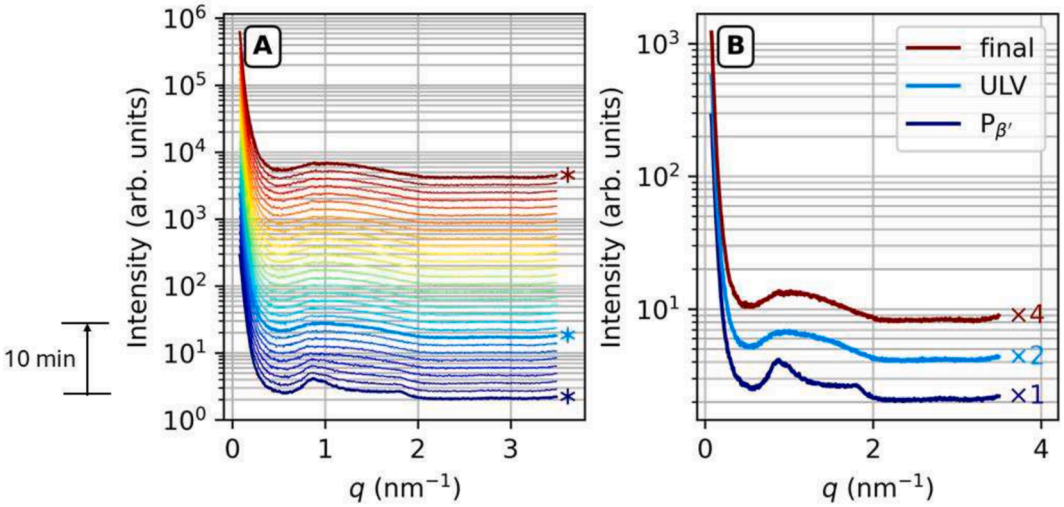

Fig. 5. Changes of the one-dimensional SAXS profiles of hydrated DPPC system (1.5 w/w%) during the sonication process at 38 °C. The whole course of transformation (A, patterns signed with asterisk are shown in B). Representative SAXS patterns (B).

3.3. ULV formation in rippled gel (38 °C) and liquid crystalline (45 °C) phases

In situ ultrasonication measurements performed at 38 °C show remarkably different changes in the nanostructure. At the very beginning, the regular SAXS pattern of the rippled gel ($P_{\beta'}$) phase is detectable (Fig. 5). The (10) reflection is dominant in the complex first Bragg peaks, corresponding to a 7.16 nm layer periodicity of the $P_{\beta'}$ phase. The second peak, consisting of (20) and (21) reflections, is broad and gets smeared out in a short time. In 10 min only the broad form factors of ULVs appeared, as it is shown separately in Fig. 5B. Extending the SAXS measurement without ultrasonication to 30 min, the shape of the scattering curve changed slightly, because a minor broad peak emerges at q = 0.8 nm^{-1}, indicating the appearance of a small amount of multilamellae beside the ULV forms.

SAXS experiments at 45 °C showed rapid structural reformations, as it can be observed in Fig. 6. Here, the shape of the regular profile of the liquid crystalline phase altered in a very short time, approx. 2 min. Afterwards, the Bragg peaks vanished, and the shape of the scattering curve continuously turned into the form factor of ULVs in approx. 3–5 min. The ultrasonication was in progress for 10 min., similarly to the previous experiment at 38 °C.

The SAXS measurement was continued for 30 min without ultrasonication. The scattering curves showed small, but tendentious changes in their profiles. Similar to the experiment performed at 38 °C, beside the apparently constant ULV form factor, a small broad Bragg reflection appeared at approx. q = 0.8 nm^{-1} at the end of the measurement series (see the separately displayed final scattering curve in Fig. 6B). Notably, this additional peak appears in a more expressed form than that at 38 °C, indicating further, unexpected structural formations. Indeed, the FF-TEM method revealed that beside the dominant small particles, large entities also occur occasionally (Fig. 7). After 10 min sonication at 45 °C and 30 min relaxation, the quenched sample contains spherical particles with typical diameters between 50–100 nm (Fig. 7A). The morphological features in the domains with negative curvature of the fractured surface, where vesicles are broken entirely through, give a direct visual information about the existence of unilamellar creations. Beside these small, spherical and apparently ULVs forms, several deviations from unilamellar formations are also revealed: fusions between ULVs, double or oligolamellar creations, small lamellar fragments packed closely to each other, or even more rarely, whole larger spherical vesicles (Fig. 7B). As the deviation from the ULV form factor is increasing with the progress of sonication (Fig. 6A), the independent FF-TEM observations indicate that prolonged ultrasonication (10 min. instead of 3–5 min.) may result in further unregular formations with defective structures during the observed relaxation time (30 min.). Consequently, the scattering contribution of these irregular formations renders the differentiation of the bilayer form factors in the different (gel, rippled gel, and liquid crystalline) phases impossible. DLS, as a further independent method also witnesses the polydisperse character of the particle size distribution of the sonicated sample, as it can be observed in Fig. 7C. The measured size distribution profile is bimodal, consisting of a sharp peak around 62.2 nm mean value, and a broad one around 649 nm in a 98 to 2 mass ratio having 0.23 and 0.52 PDI values.

3.4. Example for Applications of ULV formations of hydrated DPPC system

The previously described (section 3.3), freshly prepared ULVs of hydrated DPPC system, are typically used as precursors in the production of nanoerythrosomes. Nanoerythrosomes are promising drug-delivery systems [46,47]. When the ULVs of DPPC (formed at 45 °C under sonication) are mixed with ghost membranes prepared from human red blood cells, unilamellar vesicle-like objects, the so-called nanoerythrosomes are formed, as shown in Fig. 8 A, B, C.

The freshly prepared ghost was gently sonicated, but instead of a horn sonicator tip, a bath sonicator was used to avoid the destruction of this sensitive system. This treatment results in the fragmentation of ghost membranes into smaller parts of several hundred nm (Fig. 8B), favoring the formation of unilamellar nanoerythrosomes. These ghost fragments were mixed with the previously prepared DPPC ULVs (Fig. 8A) were extruded through porous membranes of decreasing pore size after homogenization and sonication. The FF-TEM image shows the characteristic unilamellar morphology, indicating that the ghost fragments have coated the DPPC ULVs (Fig. 8C). The scattering form factor of unilamellar constructs can be witnessed in the small-angle X-ray scattering curve of the nanoerythrosome system as a broad maximum in the q-range from 0.5 to 2 nm-1, as well as the two subsequent, lesser maxima (Fig. 8D). The decreasing, power law baseline of the scattering curve is the consequence of the small size fractions of nanoerythrosomes (which can already be observed among the precursor DPPC ULVs, Fig. 8A). Generally, the nanoerythrosomes exhibit similar SAXS curves, provided that those have similar lipid and ghost contents. The detailed inspection of the formfactors of nanoerythrosomes revealed that they have a complex unilamellar structure and the layer thickness is significantly wider than that of DPPC bilayers [48].

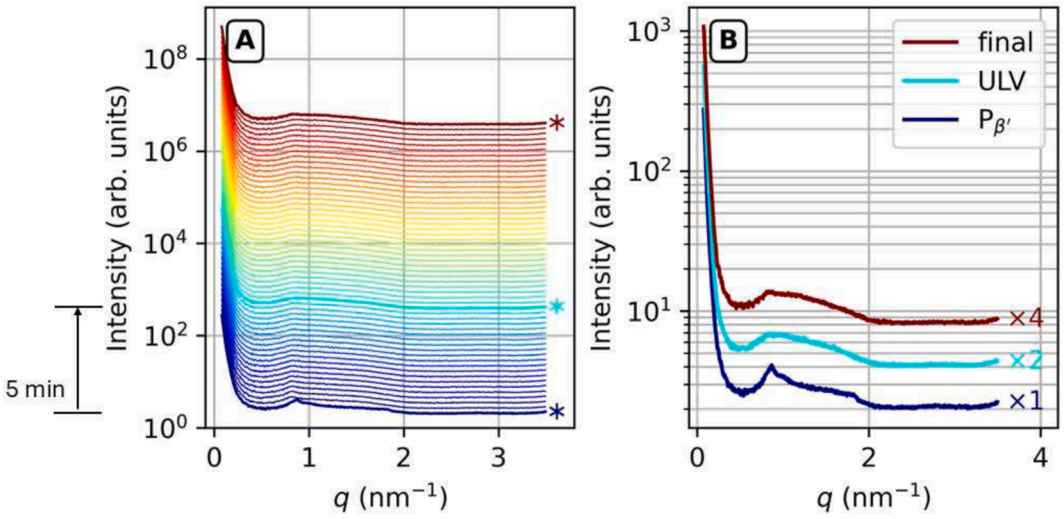

Fig. 6. Changes of the one-dimensional SAXS profiles of hydrated DPPC system (1.5 w/w%) during the sonication process at 45 °C. The whole course of transformation (A, patterns signed with asterisk are shown in B). Representative SAXS patterns (B).

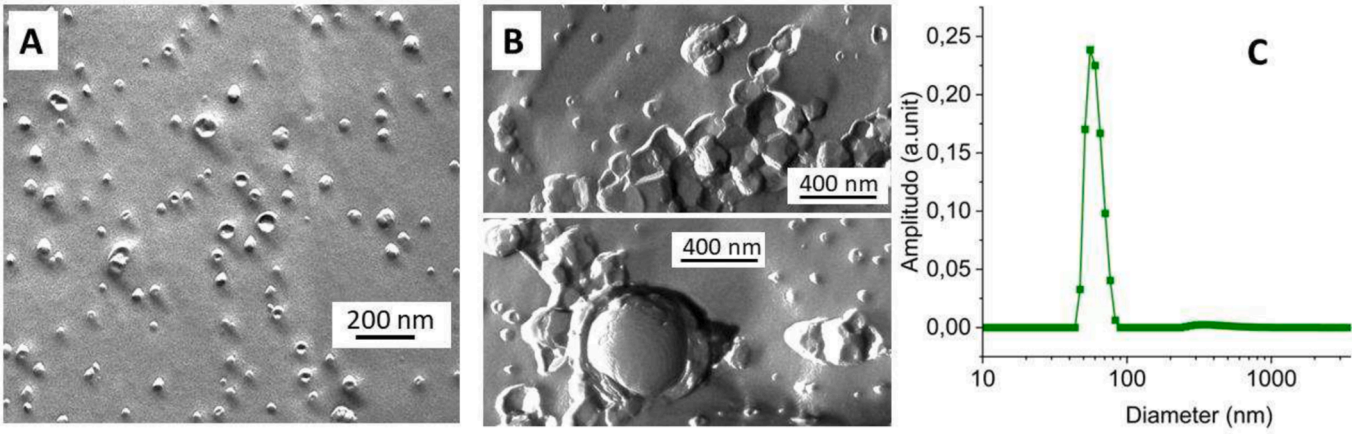

Fig. 7. Morphological changes in hydrated DPPC system (1.5 w/w%) after 10 min ultrasonication (45 °C). Nearly monodisperse ULVs (A). Beside small ULVs, irregular lamellar fragments, packed closely to each other, and polydisperse vesicle formations (B). Bimodal particle size distribution with a dominant sharp and a satellite small peak corresponding to small ULVs and large irregular creations, respectively (C).

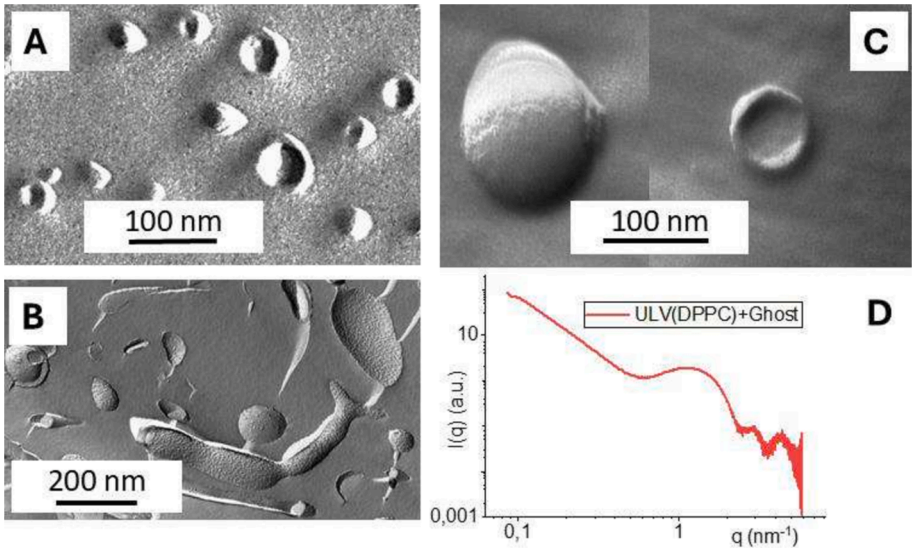

Fig. 8. Application of DPPC MLVs for nanoerythrosome-preparation. ULVs of hydrated DPPC suspension (10 min sonication, at 45 °C, A), ghost fragments (10 seconds sonication bath, B), nanoerythrosomes (20 second ultrasonication, after that extrusion through 100 nm pore size, C), SAXS pattern of ghost suspension, D).

4. Conclusion

MLVs of hydrated DPPC system, exposed to ultrasound, undergo severe structural destruction which is accompanied with the reduction of the number of bilayers in the multilayer stacks and a diminishing of the lateral size of fractured layers. In the gel phase, ensured by incubation below the pre-transition (e.g. at 20 °C), unilamellar vesicles cannot be formed. Although dynamic light scattering exhibits a relative narrow size distribution profile in the 200–300 nm range, the SAXS and FF-TEM methods revealed that bilayered phospholipid fragments are created. The formation of ULVs requires the existence of more mobile states than it is possible in the gel phase. At 38 °C, the characteristic temperatures of the thermally adjacent phases, e.g. the rippled gel and the liquid crystalline phases, are close to each other, and a minor thermal effect of ultrasound can induce main transition locally, whereby the conditions for ULV-formation comes possible. Here we found that the ultrasonication generate further structural alterations above the main transition. Although, the differentiation in the electron-micrographs is not possible which are in beginning or ending states, but the tendentious changes in SAXS pattern at 45 °C indicate that the accumulated structural defects carrying additional energy prone to create metastable creations with undesirable behaviours. Consequently, the parameters of the ultrasonication (power, time, temperature) should be carefully optimized and the prolonged ultrasonication should also be avoid. The ultrasonication, above the chain-melting transition, seems to be less advantageous than in the vicinity, but below the phase transition. As the ultrasonication without incubation may cause both the phase-transitions e.g. pre- and main transitions in the temperature domain of the gel phase which accompanied with the formations of severe structural defects and a complex prehistory, described earlier as a “memory” effect can be occurred [30]. By ultrasonication or mechanical stress induced defect structures can influence the thermotropic behaviours of the hydrated DPPC system, therefore the impact of the ultrasonication can be expected as it found recently [49]. During ultrasonication, the MLVs are influenced by localized high-pressure and −temperature zones, which induces the destruction of MLVs along their structural defects and lipid bilayer fragments (LBFs) are formed. Only the vicinity of the chain melting temperature (reached by the accumulated heat of sonication, or in a more appropriate and controllable way, through thermal incubation) assure the higher fluidity of the lipids and higher diffusion of the whole LBFs whereby ULVs can be formed, indicating the decisive role of the sonication temperature in the transformation of MLVs to ULVs, in

case of pure hydrated lipid systems.

The present SAXS results, combined with freeze-fractured electron-micrographs indicate that the formation of ULVs occur from MLVs through the forming and folding of LBFs, while the alternative process of budding from the outer surface of MLVs seems not to be likely.

CRediT authorship contribution statement

Attila Bóta: Writing – original draft, Visualization, Validation, Supervision, Resources, Project administration, Methodology, Investigation, Funding acquisition, Formal analysis, Data curation, Conceptualization. **Heinz Amenitsch:** Software, Methodology, Investigation, Formal analysis. **András Wacha:** Writing – review & editing, Visualization, Investigation, Funding acquisition, Formal analysis, Data curation.

Declaration of competing interest

The authors declare that they have no known competing financial interests or personal relationships that could have appeared to influence the work reported in this paper.

Acknowledgements

The authors are indebted to Ms Teréz Kiss for the Freeze-Fracture-TEM experiments. The project was supported by the National Research, Development and Innovation Office of Hungary under grants K131657 (A. Bóta), FK146081 (A. Wacha), and also by the Project no. 2018-1.2.1-NKP-2018-00005 under the 2018-1.2.1-NKP funding scheme (A. Bóta). A. Bóta thanks the SAXS beamtime at ELETTRA (Trieste, Italy) in the frame of CERIC-ERIC research panel (proposal id 20192058, 20212158). The Protein research program of the Hungarian Academy of Sciences (MEDinPROT, A. Bóta) is acknowledged. A. Wacha was supported by the János Bolyai Research Scholarship of the Hungarian Academy of Sciences.

Appendix A. Supplementary material

Supplementary data to this article can be found online at https://doi.org/10.1016/j.ultsonch.2024.107187.

References

[1] P. Trucillo, R. Campardelli, E. Reverchon, Liposomes: from bangham to supercritical fluids, Processes 8 (2020) 1022, https://doi.org/10.3390/pr8091022.
[2] H. Nsairat, D. Khater, U. Sayed, F. Odeh, A. Al Bawab, W. Alshaer, Liposomes: structure, composition, types, and clinical applications, Heliyon 8 (2022) e09394, https://doi.org/10.1016/j.heliyon.2022.e09394.
[3] S. Pande, Liposomes for drug delivery: review of vesicular composition, factors affecting drug release and drug loading in liposomes, Artif. Cells Nanomed. Biotechnol. 51 (2023) 428–440, https://doi.org/10.1080/21691401.2023.2247036.
[4] A.J. Guillot, M. Martínez-Navarrete, T.M. Garrigues, A. Melero, Skin drug delivery using lipid vesicles: a starting guideline for their development, J. Control. Release 355 (2023) 624–654, https://doi.org/10.1016/j.jconrel.2023.02.006.
[5] S. Dutta, J.A. Moses, C. Anandharamakrishnan, Chapter 2 - Vesicular delivery systems: applications and future trends in food technology, in: C. Anandharamakrishnan, S. Dutta (Eds.), Liposomal Encapsulation in Food Science and Technology, Academic Press, 2023, pp. 15–38, https://doi.org/10.1016/B978-0-12-823935-3.00006-0.
[6] B.S. Pattni, V.V. Chupin, V.P. Torchilin, New developments in liposomal drug delivery, Chem. Rev. 115 (2015) 10938–10966, https://doi.org/10.1021/acs.chemrev.5b00046.
[7] Y.P. Patil, S. Jadhav, Novel methods for liposome preparation, Chem. Phys. Lipids 177 (2014) 8–18, https://doi.org/10.1016/j.chemphyslip.2013.10.011.
[8] Y. Barenholzt, S. Amselem, L. D, A new method for preparation of phospholipid vesicles (liposomes) - french press, FEBS Lett. 99 (1979) 210–214, https://doi.org/10.1016/0014-5793(79)80281-1.
[9] J. Pereira-Lachataignerais, R. Pons, P. Panizza, L. Courbin, J. Rouch, O. López, Study and formation of vesicle systems with low polydispersity index by ultrasound method, Chem. Phys. Lipids 140 (2006) 88–97, https://doi.org/10.1016/j.chemphyslip.2006.01.008.
[10] R. Silva, H. Ferreira, C. Little, A. Cavaco-Paulo, Effect of ultrasound parameters for unilamellar liposome preparation, Ultrason. Sonochem. 17 (2010) 628–632, https://doi.org/10.1016/j.ultsonch.2009.10.010.
[11] C.F. De Freitas, I.R. Calori, A.L. Tessaro, W. Caetano, N. Hioka, Rapid formation of Small Unilamellar Vesicles (SUV) through low-frequency sonication: an innovative approach, Colloids Surf. B Biointerf. 181 (2019) 837–844, https://doi.org/10.1016/j.colsurfb.2019.06.027.
[12] Z.A. Nizamudeen, R. Xerri, C. Parmenter, K. Suain, R. Markus, L. Chakrabarti, V. Sottile, Low-power sonication can alter extracellular vesicle size and properties, Cells 10 (2021) 2413, https://doi.org/10.3390/cells10092413.
[13] S. Tokunaga, H. Tashiro, K. Ono, T. Sharmin, T. Kato, K. Irie, K. Mishima, T. Satho, T.M. Aida, K. Mishima, Rapid production of liposomes using high pressure carbon dioxide and direct ultrasonication, J. Supercrit. Fluids 160 (2020) 104782, https://doi.org/10.1016/j.supflu.2020.104782.
[14] H.L. Scott, A. Skinkle, E.G. Kelley, M.N. Waxham, I. Levental, F.A. Heberle, On the mechanism of bilayer separation by extrusion, or why your LUVs are not really unilamellar, Biophys. J. 117 (2019) 1381–1386, https://doi.org/10.1016/j.bpj.2019.09.006.
[15] Q. Zhong, H. Zhang, Preparation of small unilamellar vesicle liposomes using detergent dialysis method, in: G.G.M. D'Souza, H. Zhang (Eds.), Liposomes: Methods and Protocols, Springer, US, New York, NY, 2023, pp. 49–56, https://doi.org/10.1007/978-1-0716-2954-3_3.
[16] G. Du, X. Sun, Ethanol Injection Method for Liposome Preparation, in: G.G. M. D'Souza, H. Zhang (Eds.), Liposomes: Methods and Protocols, Springer, US, New York, NY, 2023, pp. 65–70, https://doi.org/10.1007/978-1-0716-2954-3_5.
[17] A. Jahn, W.N. Vreeland, M. Gaitan, L.E. Locascio, Controlled vesicle self-assembly in microfluidic channels with hydrodynamic focusing, J. Am. Chem. Soc. 126 (2004) 2674–2675, https://doi.org/10.1021/ja0318030.
[18] L. Maja, K. Željko, P. Mateja, Sustainable technologies for liposome preparation, J. Supercrit. Fluids 165 (2020) 104984, https://doi.org/10.1016/j.supflu.2020.104984.
[19] C.E. Brennen, Cavitation and bubble dynamics, Oxford University Press, New York, 1995.
[20] P. Riesz, D. Berdahl, C.L. Christman, Free radical generation by ultrasound in aqueous and nonaqueous solutions, Environ. Health Perspect. 64 (1985) 233–252, https://doi.org/10.2307/3430013.
[21] L. Rabinovich-Guilatt, C. Dubernet, K. Gaudin, G. Lambert, P. Couvreur, P. Chaminade, Phospholipid hydrolysis in a pharmaceutical emulsion assessed by physicochemical parameters and a new analytical method, Eur. J. Pharm. Biopharm. 61 (2005) 69–76, https://doi.org/10.1016/j.ejpb.2005.03.001.
[22] H.O. Hauser, The effect of ultrasonic irradiation on the chemical structure of egg lecithin, Biochem. Biophys. Res. Commun. 45 (1971) 1049–1055, https://doi.org/10.1016/0006-291X(71)90443-8.
[23] D.D. Lasic, Mechanisms of liposome formation, J. Liposome Res. 5 (1995) 431–441, https://doi.org/10.3109/08982109509010233.
[24] V.A. Bjørnestad, R. Lund, Pathways of membrane solubilization: a structural study of model lipid vesicles exposed to classical detergents, Langmuir 39 (2023) 3914–3933, https://doi.org/10.1021/acs.langmuir.2c03207.
[25] J.K. Koehler, L. Gedda, L. Wurster, J. Schnur, K. Edwards, H. Heerklotz, U. Massing, Tailoring the lamellarity of liposomes prepared by dual centrifugation, Pharmaceutics 15 (2023) 706, https://doi.org/10.3390/pharmaceutics15020706.
[26] F.A. Heberle, D. Welsch, H.L. Scott, M.N. Waxham, Optimization of cryo-electron microscopy for quantitative analysis of lipid bilayers, Biophys. Rep. 3 (2023) 100090, https://doi.org/10.1016/j.bpr.2022.100090.
[27] H.W. Meyer, W. Richter, Freeze-fracture studies on lipids and membranes, Micron 32 (2001) 615–644, https://doi.org/10.1016/S0968-4328(00)00050-0.
[28] E.A. Veschi, M. Bolean, A. Strzelecka-Kiliszek, J. Bandorowicz-Pikula, S. Pikula, T. Granjon, S. Mebarek, D. Magne, A.P. Ramos, N. Rosato, J.L. Millán, R. Buchet, M. Bottini, P. Ciancaglini, Localization of annexin A6 in matrix vesicles during physiological mineralization, Int. J. Mol. Sci. 21 (2020) 1367, https://doi.org/10.3390/ijms21041367.
[29] J.A. Zasadzinski, Transmission electron microscopy observations of sonication-induced changes in liposome structure, Biophys. J. 49 (1986) 1119–1130, https://doi.org/10.1016/S0006-3495(86)83741-9.
[30] A. Bóta, T. Drucker, M. Kriechbaum, Z. Pálfia, G. Réz, Layer formations of dipalmitoylphosphatidylcholine liposomes in the pretransition range, Langmuir 15 (1999) 3101–3108, https://doi.org/10.1021/la980507b.
[31] A. Guinier, G. Fournet, C.B. Walker, K.L. Yudowitch, Small-angle Scattering of X-rays, Wiley New York, 1955. https://www.eng.uc.edu/~beaucag/Classes/Scattering/Guinier%20and%20Fournet%20SAXS(1955).pdf (accessed October 31, 2024).
[32] P. Heftberger, B. Kollmitzer, F.A. Heberle, J. Pan, M. Rappolt, H. Amenitsch, N. Kučerka, J. Katsaras, G. Pabst, Global small-angle X-ray scattering data analysis for multilamellar vesicles: the evolution of the scattering density profile model, J. Appl. Crystallogr. 47 (2014) 173–180, https://doi.org/10.1107/S1600576713029798.
[33] A. Bóta, A. Wacha, Z. Varga, I.C. Szigyártó, S. Kristyán, A. Lőrincz, P. Szabó, M. Kálmán, L. Naszályi-Nagy, J. Mihály, Role of oligo(malic acid) on the formation of unilamellar vesicles, J. Colloid Interf. Sci. 532 (2018) 782–789, https://doi.org/10.1016/j.jcis.2018.08.020.
[34] R. Tejera-Garcia, S. Ranjan, V. Zamotin, R. Sood, P.K.J. Kinnunen, Making unilamellar liposomes using focused ultrasound, Langmuir 27 (2011) 10088–10097, https://doi.org/10.1021/la201708x.
[35] Austrian SAXS beamline at Elettra, (2021). https://www.elettra.trieste.it/elettra-beamlines/saxs.html (accessed December 9, 2021).

[36] J. Ulminus, H. Wennerstrom, G. Lindblom, G. Arvidson, Deuteron nuclear magnetic resonance studies of phase equilibriums in a lecithin-water system, Biochemistry 16 (1977) 5742–5745, https://doi.org/10.1021/bi00645a014.
[37] L. Powers, P.S. Pershan, Monodomain samples of dipalmitoyl phosphatidylcholine with varying concentrations of water and other ingredients, Biophys. J. 20 (1977) 137–152, https://doi.org/10.1016/S0006-3495(77)85540-9.
[38] H. Matsuki, M. Goto, K. Tada, N. Tamai, Thermotropic and barotropic phase behavior of phosphatidylcholine bilayers, IJMS 14 (2013) 2282–2302, https://doi.org/10.3390/ijms14022282.
[39] D. Marsh, in: Handbook of Lipid Bilayers, 2nd ed.,, CRC Press, Boca Raton, 2013, https://doi.org/10.1201/b11712.
[40] N.J. Severs, Freeze-fracture electron microscopy, Nat. Protoc. 2 (2007) 547–576, https://doi.org/10.1038/nprot.2007.55.
[41] Dynamic Light Scattering (DLS) – AvidNano W130i | CENIMAT, (2021). https://www.cenimat.fct.unl.pt/services/laboratory-electronic-and-optoelectronic-materials-and-devices/dynamic-light-scattering-dls-avidnano-w130i (accessed December 9, 2021).
[42] A. Bóta, M. Kriechbaum, Prehistory in the pretransition range of dipalmitoylphosphatidylcholine/water system, Colloids Surf. A Physicochem. Eng. Asp. 141 (1998) 441–448, https://doi.org/10.1016/S0927-7757(98)00247-7.
[43] J.F. Nagle, P. Cognet, F.G. Dupuy, S. Tristram-Nagle, Structure of gel phase DPPC determined by X-ray diffraction, Chem. Phys. Lipids 218 (2019) 168–177, https://doi.org/10.1016/j.chemphyslip.2018.12.011.
[44] H. Yao, S. Matuoka, B. Tenchov, I. Hatta, Metastable ripple phase of fully hydrated dipalmitoylphosphatidylcholine as studied by small angle x-ray scattering, Biophys. J. 59 (1991) 252–255, https://doi.org/10.1016/S0006-3495(91)82216-0.
[45] A. Bóta, A. Wacha, L. Trif, Z. Varga, J. Mihály, Limited miscibility in hydrated DPPC – Lyso-PPC systems, J. Mol. Liq. 404 (2024) 124960, https://doi.org/10.1016/j.molliq.2024.124960.
[46] S. Javed, S. Alshehri, A. Shoaib, W. Ahsan, M.H. Sultan, S.S. Alqahtani, M. Kazi, F. Shakeel, Chronicles of nanoerythrosomes: an erythrocyte-based biomimetic smart drug delivery system as a therapeutic and diagnostic tool in cancer therapy, Pharmaceutics 13 (2021) 368, https://doi.org/10.3390/pharmaceutics13030368.
[47] R. Deák, J. Mihály, I. Cs, T. Szigyártó, L. Beke-Somfai, L. Turiák, A. Drahos, A. Wacha, Z Varga Bóta, Nanoerythrosomes tailoring: Lipid induced protein scaffolding in ghost membrane derived vesicles, Mater. Sci. Eng.: C 109 (2020) 110428, https://doi.org/10.1016/j.msec.2019.110428.
[48] R. Deák, J. Mihály, I. Cs, A. Szigyártó, G. Wacha, A.B. Lelkes, Physicochemical characterization of artificial nanoerythrosomes derived from erythrocyte ghost membranes, Colloids and Surf. B: Biointerf. 135 (2015) 225–234, https://doi.org/10.1016/j.colsurfb.2015.07.066.
[49] M.D. Rieth, A. Lozano, Preparation of DPPC liposomes using probe-tip sonication: Investigating intrinsic factors affecting temperature phase transitions, Biochem. Biophys. Rep. 22 (2020) 100764, https://doi.org/10.1016/j.bbrep.2020.100764.